Published in final edited form as:
IEEE Trans Med Imaging. 2013 March ; 32(3): 628–635. doi:10.1109/TMI.2013.2239654.

Multiple Atlas Construction from A Heterogeneous Brain MR Image Collection

Yuchen Xie, **Jeffrey Ho**, and **Baba C. Vemuri [Fellow IEEE]**
Department of Computer and Information Science and Engineering (CISE), University of Florida, Gainesville, FL, 32611 USA

Baba C. Vemuri: vemuri@cise.ufl.edu

Abstract

In this paper, we propose a novel framework for computing single or multiple atlases (templates) from a large population of images. Unlike many existing methods, our proposed approach is distinguished by its emphasis on the sharpness of the computed atlases and the requirement of rotational invariance. In particular, we argue that sharp atlas images that retain crucial and important anatomical features with high fidelity are more useful for many medical imaging applications when compared with the blurry and fuzzy atlas images computed by most existing methods. The geometric notion that underlies our approach is the idea of manifold learning in a quotient space, the quotient space of the image space by the rotations. We present an extension of the existing manifold learning approach to quotient spaces by using invariant metrics, and utilizing the manifold structure for partitioning the images into more homogeneous sub-collections, each of which can be represented by a single atlas image. Specifically, we propose a three-step algorithm. First, we partition the input images into subgroups using unsupervised or semi-supervised learning methods on manifolds. Then we formulate a convex optimization problem in each subgroup to locate the atlases and determine the crucial neighbors that are used in the realization step to form the template images. We have evaluated our algorithm using whole brain MR volumes from OASIS database. Experimental results demonstrate that the atlases computed using the proposed algorithm not only discover the brain structural changes in different age groups but also preserve important structural details and generally enjoy better image sharpness.

I. Introduction

Atlases as the informative representatives of a population of images have been widely used in many medical imaging applications such as template-based image alignment [1], atlas-based image segmentation [2], [3], [4], [5] and statistical analysis across subjects [6], [7]. In addition, for heterogeneous or longitudinal data sets, multiple atlases are usually required to provide an informative and complete representation of the image data. For example, the ages of the subjects in Open Access Series of Imaging Studies (OASIS) database [8] range from 18 to 96. Since the structural difference in the brain across different age groups can be significant [9], it's not appropriate to construct a single representative atlas image for the OASIS data. Not surprisingly, algorithms and methods for computing multiple atlases from image collections have attracted considerable amount of attention recently, and in particular, the unbiased diffeomorphic atlas construction algorithm proposed in [10] has been influential for several notable recent developments such as the iCluster algorithm proposed in [11].

Correspondence to: Baba C. Vemuri, vemuri@cise.ufl.edu.

The iCluster algorithm computes multiple atlases by fitting a Gaussian mixture model to the input images. The resulting expectation-maximization algorithm (EM) iteratively groups the images into different clusters (the E-step) and computes a single atlas for images in each cluster by averaging the multiple aligned images, an approach that is similar in spirit to the unbiased diffeomorphic atlas construction algorithm. A common and visible feature of the atlas images generated by the conventional algorithms ([10], [11]) is their characteristic blurriness and the apparent absence of clear and sharp anatomical details. In short, with their characteristic lack of image fidelity, the computed atlases do not come across as real specimen of MRI images of human brains, a shortcoming that could be critical in some applications. For instance, a clear and sharp atlas is important for the accuracy of atlas-based image registration and segmentation, because it is difficult to find reliable feature correspondences between the sharp input images and a template with blurry and fuzzy structures. In the clinical setting, a characteristically clear and sharp atlas image as an informative representative of a subpopulation of patients is certainly more meaningful and accessible to medical practitioners than a fuzzy atlas image without clearly identifiable anatomical details.

This loss of image details and structures can be traced back to the atlas construction step (M-step) of the iCluster algorithm in which the atlas is computed as the arithmetic average of group-wise registered images, a popular atlas-construction paradigm first introduced in [10]. It is our observation that the unbiased diffeomorphic atlas construction algorithm often produces blurry and fuzzy atlas images unless the input images are highly homogeneous in their structures. Unfortunately, this is usually not the case and the computed atlases almost always suffer from the loss of image details in various degrees. This undesirable shortcoming can be explained in both practical and theoretical terms. In practice, the existing numerical algorithms used for computing group-wise registration cannot guarantee a globally optimal solution, and unless the images are unusually similar, non-negligible registration errors cannot be avoided in general. Coupled with the suboptimal choices of regularization constants that are often difficult to determine, it is not difficult to imagine a blurry and fuzzy atlas computed as the pixel-wise arithmetic mean of *many and inaccurately* group-wise registered images, which leads to the irreversible loss of structural details. The second and more geometric explanation can be offered as in Figure 1. The smooth variation of the input images allows us to assume (e.g., [12]) that these images belong to some smooth submanifold $\mathbf{M}$ in the ambient image space $\mathcal{I}$. Unfortunately, this manifold structure is usually difficult to model directly and perhaps more importantly, it is difficult to utilize in the group-wise registration framework. Therefore, in essence, the unbiased diffeomorphic atlas construction algorithm computes the mean of the images in the ambient image space $\mathcal{I}$, and as the figure shows, this does not guarantee that the result will be on or near the submanifold $\mathbf{M}$. This results in the loss of common image features and renders the atlas images often blurry and fuzzy.

In the context of multiple atlas construction from a large image collection, this paper proposes a novel atlas construction algorithm based on two novel conceptual improvements that aim to correct the shortcomings described above. First, unlike the EM algorithm proposed in [11], we will explicitly decouple the clustering and atlas construction steps. This decoupling provides us with greater flexibility in applying manifold learning methods (e.g., [13], [14]) to model the manifold $\mathbf{M}$, an objective that is difficult to accomplish using the traditional EM-based gaussian mixture model as in [11]. In particular, we will require that the atlas images are rotation invariant in the sense that suppose $\mathbf{I}$ is the atlas for the image collection $\{\mathbf{I}_1, \cdots, \mathbf{I}_n\}$ and if n different rotations g_i are applied to these images to form a new collection $\{g_1(\mathbf{I}_1), \cdots, g_n(\mathbf{I}_n)\}$, then the atlas $\bar{\mathbf{I}}$ for the latter collection should be related to $\mathbf{I}$ by some rotation. This technical requirement means that we can no longer assume that the input images belong to some submanifold $\mathbf{M}$ in the image space $\mathcal{I}$. Instead, the correct assumption should be that modulo rotations, the images belong to a submanifold **M** in an (abstract) quotient space **Q** of $\mathcal{I}$ [15], [16], and manifold learning provides a suitable context and natural solution for modeling **M** in this abstract setting. Furthermore, its flexibility also allows us to readily incorporate labeled images in a semi-supervised context, again an objective that would be awkward to formulate using the frameworks proposed earlier (e.g., [10], [11]). Second, we will abandon the usual paradigm of computing the atlas image as the arithmetic mean of all group-wise registered images. Instead, following the manifold assumption, we will propose a new paradigm for atlas image construction by computing the atlas as the weighted arithmetic mean of group-wise registered images. The closer an image to the true template on **M**, the larger weight it has. Figure 1 illustrates the main idea that on the manifold **M**, the mean (atlas) should be mostly determined by its neighbors as the faraway subjects have very low weights, and its computation could be formulated in a two-step process that first determines the neighbors of the abstract mean on the manifold **M** (localization) and then renders the mean as an atlas image using these neighbors (realization). In particular, these two steps utilize the input images differently: in the localization step, all images are used to determine the neighbors of the abstract mean on **M** while in the following realization step, only these neighbors are used to render the atlas image through weighted group-wise registration. To the best of our knowledge, the explicit identification and investigation of these two separate and critical processes in atlas construction have not been reported or proposed in the literature.

The proposed multiple atlas construction algorithm incorporates the ideas discussed above: A *k*-nearest neighbor graph (*k*-NN) is used to model the manifold structure of **M** [13], [14], and the graph partition algorithm is applied to the *k*-NN graph to compute clusters of the input images. Each atlas is computed as the mean of the images belong to each cluster on **M**. In general, the metric on **M** is unknown; however, the pairwise geodesic distances $d_{ij} = \mathbf{d_M}(\mathbf{I}_i, \mathbf{I}_j)$ between images can be estimated using the metric in the quotient space **Q**. An important element in the proposed algorithm is to estimate the geodesic distances $\mathbf{d_M}(\bar{\mathbf{I}}, \mathbf{I}_i)$ between the abstract mean $\bar{\mathbf{I}}$ on **M** and images $\mathbf{I}_i$ using the pairwise geodesic distances d_{ij} as the inputs. We formulate this as a convex optimization problem, and the solution to this optimization problem will provide an approximation to $\mathbf{d_M}(\bar{\mathbf{I}}, \mathbf{I}_i)$. This will allow us to locate the mean $\bar{\mathbf{I}}$ on the manifold **M** in the localization step by determining its neighbors (given a threshold). In the realization step, we use the weighted group-wise registration method to form the atlas images in each cluster given the estimated neighbors of the atlas. The proposed algorithm has been extensively evaluated and validated using OASIS data, and the experimental results have shown that, with greater preservation of important image features and details, the image atlases produced by the proposed algorithm enjoy better image sharpness and achieve higher segmentation accuracy in label propagation applications when compared with atlases obtained using exiting methods.

II. Motivation and related work

Image atlas as a standard template has been widely used for the discovery of dense correspondences between MR images of different subjects. Thus it is natural to construct the image atlas based on group-wise image registration (e.g., [10]). In this type of approach, the atlas formation is cast into an iterative energy minimization framework: input images are non-rigidly registered to a template in the common domain and the template is updated by averaging the aligned images. Unfortunately, because of the large number of variables and the non-convex cost functional, this algorithm, similar to many others, cannot avoid the prickly traps of local minima. Moreover, the rigidity of the framework makes it difficult to incorporate other useful models and information in the computation. As alluded to in the introduction, the atlas generated by this method essentially computes the atlas with respect to the the ambient image space while disregarding the potentially useful assumption of an implied manifold structure by the input images.

In recent years, manifold learning techniques have percolated into the medical image analysis community, and they have found successes in several recent works. [17] performed brain population analysis by projecting input brain images onto a low-dimensional space using Isomap [13]. [18] proposed a framework for registering images to the atlas on anatomical manifolds. Their empirical manifold is constructed from input images as a *k*-NN graph. A sample from the input population with the smallest sum of squares of geodesic distances to all input images is selected as the atlas. [19] introduced a hierarchical groupwise registration framework using the k-NN Isomap that provides the intrinsic structure of the input image dataset for their algorithm. However, all the methods discussed above construct a single atlas for the entire input image set, which implicitly assumes a homogeneous population, an assumption that is inappropriate for studying heterogeneous image data sets that are far more common and important in medical imaging analysis. iCluster is an EM-based algorithm presented by [20] for computing multiple template images for an image population. The algorithm fits a Gaussian mixture model to the input images and the input images are not assumed to possess an intrinsic manifold structure. Furthermore, it is well-known that the optimization in the EM-algorithm cannot guarantee the globally optimal solution, and therefore, good initializations of the EM-algorithm, which may not be available or even possible, are critical for the success of the method.

In this paper, we extend our previous work [21] to the multiple atlas construction problem. Several pertinent features distinguish our method from the iCluster [20] and many previously published methods. First, we use the quotient space $\mathbf{Q}$ of the image space $\mathcal{I}$ by the rotation group as the ambient image space instead of the usual image space $\mathcal{I}$ itself. Intuitively, a brain image $\mathbf{I}$ and its rotated version $\mathbf{I}'$ both represent the same subject. Thus a rotational invariant distance needs to be introduced such that the distance between $\mathbf{I}$ and $\mathbf{I}'$ is zero. Modeling the objects invariant to some group actions has been an important research topic in computer vision and medical image analysis for more than a decade. In [22], Miller and Younes introduced image metrics defined between orbits under group actions and successfully applied them to image matching. Kurtek et al. utilized q-map which is invariant under both rotation and re-parametrization groups in the shape analysis of multiple brain structures [23]. In our work, we employ a similar approach by utilizing the metric between rotation orbits in $\mathcal{I}$ to define the distance in the quotient space $\mathbf{Q}$. Second, the proposed method explicitly models the intrinsic manifold structure in the quotient space $\mathbf{Q}$ using manifold learning (*k*-NN graph) [13], [14], [24]. As illustrated in Figure 1, the image data set usually has the special structure which needs to be incorporated in the atlas construction. Moreover, we explicitly identify two important steps in the atlas formation process: localization and realization. We formulate a convex cost function in the localization step that bypasses the difficulty of globally minimizing the complicated non-convex functional, and in the realization step, we perform the weighted group-wise registration such that only a few subjects close to the mean have high weights, while the faraway subjects have very low weights in generating the atlas image. A similar idea is also presented in the recent work SharpMean [25] in which, Wu et al. developed an adaptively weighted strategy to compute the sharp group mean image which is a weighted average of the aligned subjects. Different from our method, the median image of the input subjects under Euclidean distance was chosen as the initial template and the weight of each subject for generating the group mean image was also different across the spatial locations.

III. Methods

This section presents the proposed algorithm for computing multiple atlases from a collection of images. The primary aim of our algorithm is to produce sharp atlas images that retain clear important anatomical structures common to the subpopulation of images they represent. Furthermore, we also require that the computed atlases are invariant with respect to image rotations, an important aspect of the proposed method that will be elaborated later. The strategy for achieving these two somewhat disparate goals is to utilize the notion of manifold structure implied by the images. Specifically, we will assume, as in many manifold-based learning methods (e.g.,[26], [27]), that the input images are samples from an unknown manifold $\mathbf{M}$, and the manifold structure is then modeled using a graph G computed from the input images and some metric (e.g., similarity) information among the images. The rotational invariance requirement implies that the manifold of interest $\mathbf{M}$ should be considered as a submanifold of a quotient space (quotient by the rotations), and computationally, this requires rotationally-invariant metric for computing the graph G. The graph G allows us to partition the image collection into subcollections, in both supervised and semi-supervised fashion, such that an atlas can be computed from each subcollection of images using only metrical information between the images.

Before delving into the details, we will fix the notations that will be used throughout the following discussion. Let $\mathcal{I}$ denote the space of images, and we define images in $\mathcal{I}$ formally as L^2-functions on a finite image domain $\Omega \subset \mathrm{IR}^d$ ($d = 2$ for 2D images and $d = 3$ for 3D images). Let $\mathcal{C} \equiv \{\mathbf{I}_1, \cdots, \mathbf{I}_n\}$ denote an input collection of n images and $\mathcal{A} \equiv \{\mathbf{I}a_1, \cdots, \mathbf{I}_{at}\}$the collection of t atlases for the image collection $\mathcal{C}$. A rotation $g \in \mathbf{SO}(d)$ in the image domain Ω transforms an image $\mathbf{I}$ into a rotated image $g(\mathbf{I})$ according to the formula $g(\mathbf{I})(x) = \mathbf{I}(g^{-1}(x))$ for $x \in \Omega$ and $\mathbf{I} \in \mathcal{I}$.

A. Rotational Invariance and the Geometry of the quotient space Q

The rotational invariance property described above can be formulated precisely as follows. Let $\mathcal{C}$ denote the input image collection and $\mathscr{C}' \equiv \{\mathbf{I}'_1, \cdots, \mathbf{I}'_n\}$ are images obtained by applying n rotations to images in $\mathcal{C}$: $\mathbf{I}'_i = g_i(\mathbf{I}_i)$ for $g_i \in \mathbf{SO}(d)$, $1 \le i \le n$, the atlases $\mathscr{A}' \equiv \{\mathbf{I}'_{a_1}, \cdots, \mathbf{I}'_{a_t}\}$ computed for $\mathcal{C}'$ are different from the atlases in $\mathcal{A}$ up to rotations, i.e., $\mathbf{I}'_{a_j} = r_j(\mathbf{I}_{a_j})$ for $r_j \in \mathbf{SO}(d)$, $1 \le j \le t$. The rotational invariance property requires us to work not in the image space $\mathcal{I}$ but in its quotient space $\mathbf{Q}$, the quotient space of $\mathcal{I}$ by the rotation group $\mathbf{SO}(d)$ [15], [16]. The quotient space $\mathbf{Q}$ is a space that parameterizes the $\mathbf{SO}(d)$-orbits in $\mathcal{I}$ and in this paper, we will assume that $\mathbf{Q}$ has a manifold structure induced from the manifold structure of $\mathcal{I}$. Let $\boldsymbol{\pi} : \mathcal{I} \to \mathbf{Q}$ denote the canonical projection map that sends each image $\mathbf{I} \in \mathcal{I}$ to the unique $\mathbf{SO}(d)$-orbit $[\mathbf{I}] \in \mathbf{Q}$ containing $\mathbf{I}$: $\boldsymbol{\pi}(\mathbf{I}) = [\mathbf{I}]$.

There is a well-known bijective correspondence [16] between metrics on $\mathbf{Q}$ and $\mathbf{SO}(d)$-invariant metric on $\mathcal{I}$. Recall that a $\mathbf{SO}(d)$-invariant metric on $\mathcal{I}$ satisfies the following condition

$$\mathbf{d}_{\mathscr{I}}(\mathbf{I}_1, \mathbf{I}_2) = \mathbf{d}_{\mathscr{I}}(g(\mathbf{I}_1), g(\mathbf{I}_2)),$$

for any two images $\mathbf{I}_1, \mathbf{I}_2 \in \mathcal{I}$ and $g \in \mathbf{SO}(d)$. The correspondence between metrics $\mathbf{d}_\mathbf{Q}$ on $\mathbf{Q}$ and $\mathbf{SO}(d)$-invariant metrics $\mathbf{d}_\mathcal{I}(x, y)$ on $\mathcal{I}$ is provided by the formula [16],

$$\mathbf{d}_{\mathbf{Q}}([\mathbf{I}_1],[\mathbf{I}_2])=\min_{x\in[\mathbf{I}_1],y\in[\mathbf{I}_2]}\mathbf{d}_{\mathscr{I}}(x,y), \quad (1)$$

for any two points $[\mathbf{I}_1], [\mathbf{I}_2] \in \mathbf{Q}$. Note that $[\mathbf{I}_1], [\mathbf{I}_2]$ are realized in $\mathcal{I}$ as $\mathbf{SO}(d)$-orbits, and $\mathbf{d}_{\mathbf{Q}}$ simply computes the distance between the two orbits in $\mathcal{I}$ as measured by $\mathbf{d}_{\mathcal{I}}$ in $\mathcal{I}$. Because of the property of $\mathbf{SO}(d)$-invariant metrics, $\mathbf{d}_{\mathbf{Q}}$ can be computed with respect to only one transformation instead of a rotation per each orbit.

$$\begin{aligned}\mathbf{d}_{\mathbf{Q}}([\mathbf{I}_1],[\mathbf{I}_2])&=\min_{g_1,g_2\in\mathbf{SO}(d)}\mathbf{d}_{\mathscr{I}}(g_1(\mathbf{I}_1),g_2(\mathbf{I}_2))\\&=\min_{g_1,g_2\in\mathbf{SO}(d)}\mathbf{d}_{\mathscr{I}}(g_2^{-1}\circ g_1(\mathbf{I}_1),g_2^{-1}\circ g_2(\mathbf{I}_2))\\&=\min_{g\in\mathbf{SO}(d)}\mathbf{d}_{\mathscr{I}}(g(\mathbf{I}_1),\mathbf{I}_2).\end{aligned} \quad (2)$$

The two related metrics $\mathbf{d}_{\mathcal{I}}$, $\mathbf{d}_{\mathbf{Q}}$ allows us to go between $\mathcal{I}$ and $\mathbf{Q}$. In particular, any computation relating to a metric on $\mathbf{Q}$ can be equivalently formulated using its corresponding $\mathbf{SO}(d)$-invariant metric on $\mathcal{I}$. Fortunately, many metrics in $\mathcal{I}$ can be easily shown to be $\mathbf{SO}(d)$-invariant, such as the usual L^2-metric and the following metric proposed in [12]:

$$\mathbf{d}_{\mathscr{I}}(\mathbf{I}_1,\mathbf{I}_2)=\min_{h_i}\left(\int_{\Omega}|\mathbf{I}_1(h_i(x))-\mathbf{I}_2|^2dx+\int_0^1\int_{\Omega}\left\|Lv_i\right\|^2dxds\right)^{1/2} \quad (3)$$

where v_i is the time-dependent vector field that defines the diffeomorphic flow from the identity to the diffeomorphism h_i, and L is a second-order elliptic operator. The metric in (3) can be computed by using nonrigid diffeomorphic image registration. Given the images $\mathbf{I}_i$ in $\mathcal{C}$, the manifold $\mathbf{M}$ that will be modeled pertains to the points $\{[\mathbf{I}_1], \cdots, [\mathbf{I}_n]\}$ in the quotient space $\mathbf{Q}$. As a submanifold of $\mathbf{Q}$, $\mathbf{M}$ is naturally equipped with the induced Riemannian metric, and in the following, we will denote $\mathbf{d}_{\mathbf{M}}([\mathbf{I}_i], [\mathbf{I}_j])$ the geodesic distance function on $\mathbf{M}$.

B. Graph representation of the manifold M

Because the manifold $\mathbf{M}$ does not have explicit representation, we follow the common approach that uses a graph $G = (V, E)$ to characterize its manifold structure, where V, E are the node and edge sets, respectively. In this construction, the node set $V = \{[\mathbf{I}_1], \cdots, [\mathbf{I}_n]\}$ is provided by the points $[\mathbf{I}_i]$ in the quotient space $\mathbf{Q}$. The edge set E that defines the connectivity of G is determined by the pair-wise distances among the points $[\mathbf{I}_i]$ via the standard k-nearest neighbor (k-NN) construction. That is, an edge is formed between every node and its k nearest neighbors. A simple example is shown in Figure 1, and in this example, each node is connected to its two nearest neighbors ($k = 2$) and the resulting graph gives a good approximation to the underlying curve.

Because of the heterogeneity of some image sets, we partition the graph G into t subgraphs in order to compute multiple atlases to represent the image sets. Spectral clustering and related methods provide a readily available algorithms for partitioning the graph G. Popular and well-known algorithms include Ratio Cut [28] and Normalized Cut [29], and our unsupervised graph partition algorithm based on Normalized Cut is outlined in Algorithm 1. The algorithm partitions the graph using the graph Laplacian matrix $\mathbf{L}$ that is computed from the similarity matrix $\mathbf{W}$ that encodes all the metrical information provided by the nodes $[\mathbf{I}_i]$:

$$W_{ij}=\begin{cases} \exp(-\frac{\mathbf{d_Q}([\mathbf{I}_i],[\mathbf{I}_j])^2}{\sigma^2}) & \text{if } j \in \mathcal{N}_i \text{ or } i \in \mathcal{N}_j, \\ 0 & \text{otherwise,} \end{cases} \quad (4)$$

where $\mathcal{N}_i$ and $\mathcal{N}_j$ are k nearest neighborhoods. The parameter $\boldsymbol{\sigma}$ is empirically estimated by $\sigma=\frac{1}{n}\sum_{i=1}^{n}\mathbf{d_Q}([\mathbf{I}_i],[\mathbf{I}_{i_k}])$ where $[\mathbf{I}_{i_k}]$is the k-th nearest neighbor of $[\mathbf{I}_i]$. The graph Laplacian matrix is defined as

$$\mathbf{L}=\mathbf{D}-\mathbf{W} \quad (5)$$

where $\mathbf{D}$ is an $n \times n$ diagonal matrix with $D_{ii}=\sum_{j=1}^{n}W_{ij}$.

After the partition, we obtain t subgraphs $G_i = (V_i, E_i)$, where $V_1, \ldots, V_t$ is the partition of the set V and $E_i \subset E$ only includes edges whose two vertices are in V_i. The number of clusters t is usually set manually by most spectral clustering algorithms. In [30], Zelnik-Manor and Perona suggested an approach to optimally select the number of clusters by analyzing the eigenvectors of the graph Laplacian matrix $\mathbf{L}$. For each possible cluster number, the best rotation is recovered to align the eigenvector matrix with the canonical coordinate system. The optimal number of clusters t is then set as the cluster number with minimal alignment cost.

The above unsupervised framework can be easily extended to a semi-supervised framework with partially labeled data. This extension is relevant because in many medical imaging applications, a small number of data labeled by experts are usually available, and they should be utilized to improve the analysis and classification of the remaining unlabeled data. Inspired by the ideas from semi-supervised learning [26], [27], we consider the graph partition problem with partially labeled nodes as a classification problem that transfers the known labels to the unlabeled data.

We will consider the two-class partition problem with the label set $Y = \{-1, 1\}$ at first. It can be formulated as a binary classification problem on the manifold with the classifier defined as a function: $f: \mathbf{M} \to Y$. When $\mathbf{M}$ is a compact manifold, the eigenfunctions of the Laplace-Beltrami operator Δ provide a natural orthogonal basis for the Hilbert space $L^2(\mathbf{M})$ [27]. That means any function $f \in L^2(\mathbf{M})$ can be written in terms of the eigenfunctions of Δ:

$$f(x)=\sum_{i=1}^{\infty}a_i u_i(x), \quad (6)$$

where a_i are coefficients and u_i are eigenfunctions such that $\Delta u_i = \lambda_i u_i$. Thus we could fit the classifier on the labeled data and find the optimal model parameters $\mathbf{a}$ which will be used to classify the unlabeled data. Let the sample set be $\mathcal{X} = \{x_1, \ldots, x_s, x_{s+1}, \ldots, x_n\} \subset \mathbf{M}$. Without loss of generality, we assume the first s data are labeled and others are unlabeled. The label set is $\{c_1, \ldots, c_s\}$, where $c_i \in Y$. Given the graph Laplacian $\mathbf{L}$, we can solve the eigenvector problem $\mathbf{Lu} = \lambda\mathbf{u}$ to generate the corresponding eigenfunctions. Let $\mathbf{u}_1, \ldots, \mathbf{u}_p$ be eigenvectors corresponding to the p smallest eigenvalues. $\mathbf{u}_i = [u_{i1}, \ldots, u_{in}]^T$, where $i = 1, \ldots, p$. Then we are able to train the classifier from the labeled data by minimizing the following cost function

$$\mathscr{E}(\mathbf{a})=\sum_{i=1}^{s}\left(c_i-\sum_{j=1}^{p}a_j u_{ji}\right)^2=\left\|\mathbf{U}\mathbf{a}-\mathbf{c}\right\|^2, \quad (7)$$

where the coefficients $\mathbf{a} = [a_1, \dots, a_p]^T$, the labels $\mathbf{c} = [c_1, \dots, c_s]^T$ and the basis matrix $\mathbf{U}=\begin{pmatrix} u_{11} & \cdots & u_{p1} \\ \vdots & \ddots & \vdots \\ u_{1s} & \cdots & u_{ps} \end{pmatrix}$.

The closed-form solution of this optimization problem is $\mathbf{a} = (\mathbf{U}^T\mathbf{U})^{-1}\mathbf{U}^T\mathbf{c}$. For the unlabeled data x_i, $i > s$, we just apply the trained classifier and set the label to be 1 if $\sum_{j=1}^{p} a_j u_{ji} \geq 0$, otherwise the label is set to −1. For t-classes graph partition, $t > 2$, we follow the *one-versus-the-rest* approach which is commonly used in multiclass support vector machines [31]. We build t separate two-class classifiers f_k, where $k = 1, \dots, t$. The k-th classifier is estimated by using the data from class-k as the positive samples and the data from remaining $t-1$ classes as the negative samples. Then t coefficients $\mathbf{a}_k = [a_{k1}, \dots, a_{kp}]^T$, $1 \leq k \leq t$ are computed and will be used to classify unlabeled data. For x_i, $i > s$, the label is set to be $\arg\max_k f_k(x_i)=\sum_{j=1}^{p} a_{kj} u_{ji}$. This multi-class semi-supervised graph partition algorithm is summarized in Algorithm 2.

C. Estimating mean from pairwise geodesic distances

After the graph partition, we need to construct an atlas for each subgraph. Without loss of generality, we suppose $\{x_1, \cdots, x_n\}$ are nodes of one subgraph G_a on a manifold $\mathbf{M}$. Let $\bar{x} \in \mathbf{M}$ denote the mean of points $\{x_1, \cdots, x_n\}$ on $\mathbf{M}$ and $\mathbf{d_M}$ denotes the Riemannian geodesic distance on $\mathbf{M}$. Although we do not have the analytic representation for $\mathbf{d_M}$, we could approximate $\mathbf{d_M}(x_i, x_j)$, $1 \leq i, j \leq n$ with $\mathbf{d_Q}$ and the graph structure of G_a. For each edge $(x_p, x_q) \in E_a$, let the distance $\mathbf{d_Q}(x_p, x_q)$ be its weight. Because a geodesic is defined as the shortest path between two points on the manifold, inspired by the approach in ISOMAP [13], we could use Dijkstra's algorithm or the Floyd-Warshall algorithm [32] to find the shortest path between two nodes x_i, x_j on the graph and use it to approximate the geodesic on the manifold $\mathbf{M}$. One possible way to determine the mean $\bar{x}$ is the following. Let $a_i = \mathbf{d_M}(x_i, \bar{x})$, $1 \leq i \leq n$. Determining a_i is of course equivalent to locating $\bar{x}$ on $\mathbf{M}$, and a_i can be determined as the solution to an optimization problem given by:

$$\begin{array}{ll} \min & a_1^2+a_2^2+\cdots+a_n^2 \\ \text{s.t.} & a_i \geq 0, \ \ i=1,\cdots n \\ & a_i+a_j \geq \mathbf{d}_{\mathbf{M}}(x_i, x_j), \\ & a_i+\mathbf{d}_{\mathbf{M}}(x_i, x_j) \geq a_j, \\ & a_j+\mathbf{d}_{\mathbf{M}}(x_i, x_j) \geq a_i, i, j=1,\cdots n. \end{array} \quad (9)$$

The linear inequality constraints between a_i and $\mathbf{d_M}(x_i, x_j)$ are imposed because $\mathbf{d_M}$ satisfies the triangle inequality [33]. For our problem, the manifold $\mathbf{M}$ and its metric $\mathbf{d_M}$ are unknown, and consequently, the higher-degree constraints cannot be known. Thus only linear constraints are considered in this paper.

The optimization problem is clearly convex since the objective function is strictly convex (the Hessian is positive-definite everywhere) and the domain, which is the intersection of half-spaces, is also convex. This particular type of optimization problem (with quadratic cost function and linear inequality constraints) can be solved efficiently even with a large number of variables and constraints. And because the objective function is strictly convex, the solution is unique [34]. Furthermore, the solution is stable with respect to the input parameters $\mathbf{d_M}(x_i, x_j)$ in the sense that small perturbations of $\mathbf{d_M}(x_i, x_j)$ will not significantly alter the solution $a_1, \cdots, a_n$ [34]. The quadratic programming problem in (9) is special in that the Hessian in the objective function is just a diagonal matrix and the constraint matrix is sparse. Therefore, in our experiments, we choose the interior point method which can handle large-scale quadratic optimization problem. For computing robust $\mathbf{L}^1$-median [35] instead of mean, we simply need to change the cost function to $a_1 + a_2 + \cdots + a_n$.

D. Computing the image atlases

The result of the previous localization step provides us with the pairwise distances $\mathbf{d_M}([\bar{\mathbf{I}}], [\mathbf{I}_i])$, and at this point, the atlas has been located only in the abstract manifold $\mathbf{M}$ in terms of these distances. In the realization step, we will render the atlas image using the distance data $\mathbf{d_M}([\bar{\mathbf{I}}], [\mathbf{I}_i])$ and the input images. Specifically, given the vertex set $\{[\mathbf{I}_1], \cdots, [\mathbf{I}_n]\}$ of subgraph G_a and the corresponding non-negative numbers a_i as estimates on the geodesic distances $\mathbf{d_M}([\bar{\mathbf{I}}], [\mathbf{I}_i])$, where $i = 1, \ldots, n$, we realize the image atlas using a weighted group-wise registration approach. Because the closer a sample image to the atlas on the manifold $\mathbf{M}$, the more contribution it will give in atlas realization, the weight is in the form of an exponential function $\exp(-a_i^2/\sigma^2)$. Given the k-NN graph, σ is empirically estimated by the kth smallest a_i. Since the weight will be close to 0 if a_i is large, we determine K points in $\{[\mathbf{I}_1], \cdots, [\mathbf{I}_n]\}$ that are close to $[\bar{\mathbf{I}}]$ as measured by $\mathbf{d_M}$, and the atlas image is then approximated from these points with respect to the metric $\mathbf{d_Q}$ in $\mathbf{Q}$. In practice, a positive integer K is specified such that the sum of weights of K points $[\mathbf{I}_{i_1}], \cdots, [\mathbf{I}_{i_K}]$ with shortest distances to $[\bar{\mathbf{I}}]$ covers more than 95% of the total weight.

We could approximate $[\bar{\mathbf{I}}]$ by solving the following optimization problem:

$$[\bar{\mathbf{I}}]=\underset{[\mathbf{I}']\in\mathbf{Q}}{\operatorname{argmin}}\sum_{j=1}^{K} w_j \mathbf{d}_{\mathbf{Q}}^2([\mathbf{I}_{i_j}], [\mathbf{I}']). \quad (10)$$

w_j can be constructed from the estimated geodesic distances a_{i_j}:

$$w_j = b_j \Big/ \left(\sum_{k=1}^{K} b_k\right)$$

where $b_j=\exp(-a_{i_j}^2/\sigma^2),\ 1 \le j \le K$. Using the metric defined by equation (3), the corresponding atlas $\bar{\mathbf{I}}$ is computed by solving the variational problem

$$\min_{\bar{\mathbf{I}}, h_j, g_j} \sum_{j=1}^{K} w_j \left(\int_\Omega |\mathbf{I}_{i_j}(h_j g_j(x)) - \bar{\mathbf{I}}|^2 dx + \int_0^1 \int_\Omega \left\| L v_j \right\|^2 dx ds \right) \quad (11)$$

where $g_j \in \mathbf{SO}(d)$, h_j is diffeomorphism and L is a second-order elliptic operator. We use an iterative approach to solve the above problem. In each iteration, the input images are group-wise aligned by rotations and then a weighted nonrigid group-wise registration is applied. The atlas image is updated as the weighted average of the registered input images. Overall, our multiple atlases construction approach is outlined in Algorithm 3.

IV. Experiments

In this section, we apply the proposed algorithms to compute atlases from collections of MR images and compare with the conventional image atlas construction methods ANTS [36] and iCluster [11], [20] respectively. Specifically, the image data used in our experiment are the MR images from the freely available Open Access Series of Imaging Studies (OASIS) dataset [8]. OASIS contains T1 weighted MR brain images from a cross-sectional population of 416 subjects. Each MR scan has the size of 176×208×176 voxels and the resolution of $1 \times 1 \times 1\ mm^3$. The ages of the subjects range from 18 to 96. For each subject, a label image with segmentations of white matter (WM), gray matter (GM) and cerebrospinal fluid (CSF) is also provided.

A. Single atlas for OASIS data

In the first experiment, we evaluated the performance of our graph-based single atlas construction method. For comparison, we employed the image template construction method provided by Advanced Normalization Tools (ANTS), which is a state-of-the-art ITK-based toolkit for computational anatomy. The atlas construction method in ANTS is alike the conventional group-wise image registration approach presented in [10]. The atlas is iteratively generated by registering the input images to the latest group mean and then averaging the warped subjects. We used symmetric diffeomorphic transformation and the mean squared similarity measure in our experiment. 50 subjects across different ages were selected from the OASIS dataset for the atlas construction. The image atlases constructed by the proposed method and ANTS are shown in Figure 2. It's clear from the figure that our sharp image template preserves better the subtle anatomical structures than the "fuzzy" mean image generated by the conventional atlas construction method in ANTS.

In order to quantitatively evaluate the effectiveness of the proposed atlas construction method, we also conducted an experiment on atlas based image segmentation. Since the deformation of each input image to the atlas is computed, the corresponding WM/GM/CSF label map can be warped to the reference domain. We set the tissue label of the image atlas at each voxel as the majority of tissue assignments from all registered images. Then the image template with the tissue label map was warped to 10 additional OASIS subjects to achieve the atlas based tissue segmentation. We used the DICE score to quantitatively measure the segmentation accuracy. The segmentation DICE scores of white matter (WM), gray matter (GM) and cerebrospinal fluid (CSF) for the ten OASIS subjects are displayed in Figure 3. In this atlas based segmentation application, the image atlas constructed by the proposed method consistently achieves better segmentation accuracy than the mean image template generated by ANTS, with the overall average DICE score 0.7769 by our method and 0.7420 by ANTS.

B. Multiple atlases for OASIS data

Because the structural difference in the brain across different age groups can be significant [9], the OASIS data set is far from homogeneous. Therefore, instead of a single mean template image, multiple atlases are required to represent the whole OASIS data satisfactorily.

In the first part of this experiment, we constructed two atlases for the collection of 416 subjects in the OASIS dataset using both the unsupervised and semi-supervised methods. In all following experiments, we set $k = 10$ when constructing the k-NN graphs. For the unsupervised graph partition, we use two clusters, and for the semi-supervised graph partition, we randomly choose 20 subjects younger than 50 years old and 20 subjects older than or equal to 50 as the labeled samples. The remaining subjects are considered as unlabeled samples. Table I compares the means and standard deviations of ages of subjects in the two clusters computed by EM-based iCluster algorithm [20], our unsupervised and semi-supervised methods. The means and standard deviations of two age groups separated by 50 are also listed in Table I as a reference. The clustering result of our unsupervised method is similar to iCluster, while our semi-supervised method gives slightly smaller mean ages for both young and old groups.

The partial labels in semi-supervised learning provide useful information to correctly classify more subjects aged between 50 and 70 into the older group. As shown in Figure 4, the atlases generated by iCluster are blurry, while the atlases computed by our methods are substantially sharper, retaining more structural details. This is not surprising because our atlases are computed as means on the manifolds, instead of the means in the ambient space. The age histogram also reveals that a third cluster for middle-aged subjects can be defined for the OASIS cross-sectional set. Accordingly, in the second experiment, we used three clusters for our unsupervised atlases construction algorithm. For the semi-supervised algorithm, we first divided the OASIS population into three groups: young (subjects younger than 40), middle-aged (between 40 and 60) and older adults (older than 60). The means and standard deviations of ages of subjects in these three pre-determined groups are displayed in Table II. Then we randomly sampled 20 subjects from each group as the labeled data and considered the remainder unlabeled. The histograms of both unsupervised and semi-supervised partition results are shown in Figure 5. For our unsupervised method, the middle-aged cluster has a significant overlap with the old cluster, and a similar result was also reported in [20]. The clustering methods employed by both algorithms are designed to detect and discover the dominant structural modes, and there is an obvious structural difference between old (around 60) and elderly (around 75) subjects. This complicates the task of determining the middle-age mode in the age distribution using these clustering techniques. However, since the semi-supervised method uses more information from partially labeled data, it gives a better classification for different modes in the age distribution. Table II compares the means and standard deviations of ages of subjects in all three classes computed by iCluster, our unsupervised and semi-supervised methods, and Figure 6 shows the corresponding atlases constructed by these three algorithms. The clustering result of our unsupervised method is similar to iCluster, but our method provides considerably sharper atlases, which are very useful in applications such as atlas-based segmentation and tensor-based morphometry. Compared with corresponding mean ages computed by iCluster and our unsupervised methods, the mean age of class two computed by our semi-supervised partition method is 54.6, which is substantially closer to the mode for the middle-aged group one would expect from the histogram of the age distribution.

With the age information for some subjects, our semi-supervised method has the ability to construct more than three atlases across ages, which is akin to the population shape regression [12]. The regression method requires ages of all subjects in the data set, while our method only needs class labels for a small number of images. The OASIS data can be partitioned into seven classes with ten years interval. We randomly chose ten subjects from each class as the labeled data and consider the remaining unlabeled. Note that only 16.8% of images are labeled. The atlases computed across seven different age groups in the OASIS data are shown in Figure 7. All atlases are sharp with many clearly visible structural details, and in particular, the progressive enlargement of the ventricle with aging can be observed clearly in the atlas sequence and the accelerated expansion of the ventricle after age sixty shown in the atlas sequence corroborates with the findings reported in [9] and [12].

V. Conclusion

We have proposed a novel approach to the multiple atlas construction problem. Compared with many algorithms published in literature for achieving this task, the novel point advocated in this paper is the importance of having sharp atlas images that retain clear structural details common among the input images. For large image collections, which typically contain substantial structural heterogeneity, the proposed two-step approach achieves the above stated aim by first partitioning the image collection into (relatively) more homogeneous subcollections followed by a novel atlas construction algorithm that explicitly computes a single image atlas for each sub-collection of images. We have provided several experimental results that validate the proposed algorithm, and in particular, comparisons with existing methods have shown that the atlases computed using the proposed algorithm enjoy better image sharpness with better preservation of important image features and details.

Acknowledgments

This research was in part supported by the NIH grant NS066340 to BCV, and the NSF grant IIS 0916001 to JH and BCV.

References

1. Talairach, J.; Tournoux, P. Co-planar stereotaxic atlas of the human brain. Vol. 147. Thieme; New York: 1988.
2. Vemuri B, Ye J, Chen Y, Leonard C. Image registration via level-set motion: Applications to atlas-based segmentation. Medical image analysis. 2003; 7(1):1–20. [PubMed: 12467719]
3. Fischl B, et al. Whole Brain Segmentation:: Automated Labeling of Neuroanatomical Structures in the Human Brain. Neuron. 2002; 33(3):341–355. [PubMed: 11832223]
4. Bazin P, Pham D. Statistical and topological atlas based brain image segmentation," in. MICCAI. 2007:94–101. [PubMed: 18051048]
5. Thomas Yeo B, Sabuncu M, Desikan R, Fischl B, Golland P. Effects of registration regularization and atlas sharpness on segmentation accuracy. Medical Image Analysis. 2008; 12(5):603–615. [PubMed: 18667352]
6. Ashburner J, Hutton C, Frackowiak R, Johnsrude I, Price C, Friston K. Identifying global anatomical differences: deformation-based morphometry. Human Brain Mapping. 1998; 6(5–6): 348–357. [PubMed: 9788071]
7. Hua X, et al. Tensor-based morphometry as a neuroimaging biomarker for Alzheimer's disease: an MRI study of 676 AD, MCI, and normal subjects. Neuroimage. 2008; 43(3):458–469. [PubMed: 18691658]
8. Marcus D, Wang T, Parker J, Gsernansky J, Morris J, Buckner R. Open access series of imaging studies (oasis): Cross-section mri data in young, middle aged, nondemented, and demented older adults. Journal of Cognitive Neuroscience. 2007; 19:1498–1507. [PubMed: 17714011]
9. Mortamet B, Zeng D, Gerig G, Prastawa M, Bullitt E. Effects of healthy aging measured by intracranial compartment volumes using a designed mr brain database," in. MICCAI. 2005
10. Joshi S, Davis B, Jomier M, Gerig G. Unbiased diffeomorphic atlas construction for computational anatomy. NeuroImage. 2004; 23:S151–S160. [PubMed: 15501084]
11. Sabuncu M, Balci S, Golland P. Discovering modes of an image population through mixture modeling," in. MICCAI. 2008
12. Davis B, Fletcher P, Bullitt E, Joshi S. Population shape regression from random design data," in. ICCV. 2007
13. Tenenbaum J, de Silva V, Langford J. A global geometric framework for nonlinear dimensionality reduction. Science. 2000; 290(5500):2319–2323. [PubMed: 11125149]
14. Belkin M, Niyogi P. Laplacian eigenmaps and spectral techniques for embedding and clustering. NIPS. 2002; 1:585–592.

15. Munkres, J. Topology. Prentice Hall; 2000.
16. Mumford, D.; Fogarty, J.; Kirwan, F. Geometric Invariant Theory. Springer; 1994.
17. Gerber S, Tasdizen T, Thomas Fletcher P, Joshi S, Whitaker R. Manifold modeling for brain population analysis. Medical Image Analysis. 2010; 14(5):643–653. [PubMed: 20579930]
18. Hamm J, Ye D, Verma R, Davatzikos C. GRAM: A framework for geodesic registration on anatomical manifolds. Medical Image Analysis. 2010; 14(5):633–642. [PubMed: 20580597]
19. Jia H, Wu G, Wang Q, Shen D. ABSORB: Atlas building by self-organized registration and bundling. NeuroImage. 2010; 51(3):1057–1070. [PubMed: 20226255]
20. Sabuncu M, Balci S, Shenton M, Golland P. Image-driven population analysis through mixture modeling. IEEE Transactions on Medical Imaging. 2009; 28(9):1473–1487. [PubMed: 19336293]
21. Xie Y, Ho J, Vemuri B. Image atlas construction via intrinsic averaging on the manifold of images," in. CVPR. 2010
22. Miller M, Younes L. Group actions, homeomorphisms and matching: a general framework. International Journal of Computer Vision. 2001; 41:61–84.
23. Kurtek S, et al. Parameterization-invariant shape comparisons of anatomical surfaces. IEEE Transactions on Medical Imaging. 2011; 30(3):849–858. [PubMed: 21156390]
24. Belkin M, Niyogi P. Using manifold structure for partially labeled classification," in. NIPS. 2002
25. Wu G, Jia H, Wang Q, Shen D. Sharpmean: Groupwise registration guided by sharp mean image and tree-based registration. NeuroImage. 2011
26. Zhu, X. Technical Report 1530 Department of Computer Science. University of Wisconsin; Madison: 2005. Semi-supervised learning literature survey.
27. Belkin M, Niyogi P. Semi-supervised learning on Riemannian manifolds. Machine Learning. 2004; 56(1):209–239.
28. Hagen L, Kahng A. New spectral methods for ratio cut partitioning and clustering. IEEE Transactions on Computer-Aided Design of Integrated Circuits and Systems. 1992; 11(9):1074–1085.
29. Shi J, Malik J. Normalized cuts and image segmentation. IEEE Transactions on Pattern Analysis and Machine Intelligence. 2000; 22(8):888–905.
30. Zelnik-Manor L, Perona P. Self-tuning spectral clustering. NIPS. 2004; 17:1601–1608.
31. Vapnik, V. Statistical learning theory. Wiley; New York: 1998.
32. Cormen, T.; Leiserson, C.; Rivest, R.; Stein, C. Introduction to algorithms. The MIT press; 2001.
33. Karcher H. Riemannian centers of mass and mollifier smoothing. Comm on Pure and Appl Math. 1977; 30:509–541.
34. Boyd, A.; Vandenberghe, L. Convex Optimization. Cambridge University Press; 2004.
35. Fletcher P, Venkatasubramanian S, Joshi S. Robust statistics on riemannian manifold via the geometric median," in. CVPR. 2008
36. Avants B, Tustison N, Song G, Cook P, Klein A, Gee J. A reproducible evaluation of ants similarity metric performance in brain image registration. Neuroimage. 2011; 54(3):2033–2044. [PubMed: 20851191]

NIH-PA Author Manuscript
NIH-PA Author Manuscript

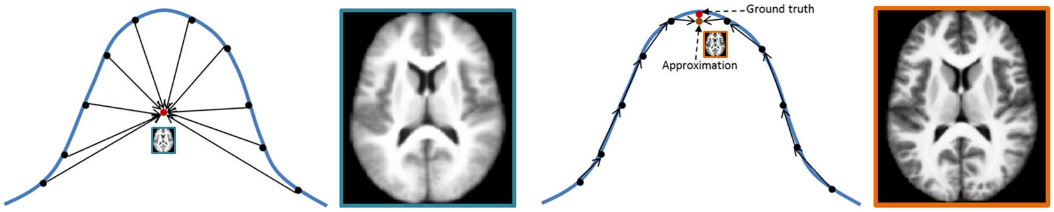

Fig. 1.
Ten points on an one-dimensional manifold. **Left:** Mean for the ten points computed using the metric of the ambient space (iCluster). **Right:** Mean computed using the metric of the submanifold **M** (the proposed method). Notice the greater preservation of image features and structures of the right atlas.

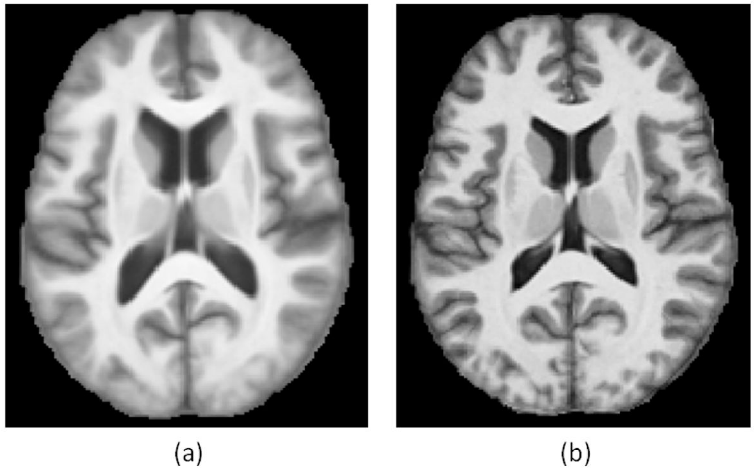

Fig. 2.
Axial view of constructed image atlases. **(a)**: Atlas generated using ANTS. **(b)**: Atlas generated using the proposed method.

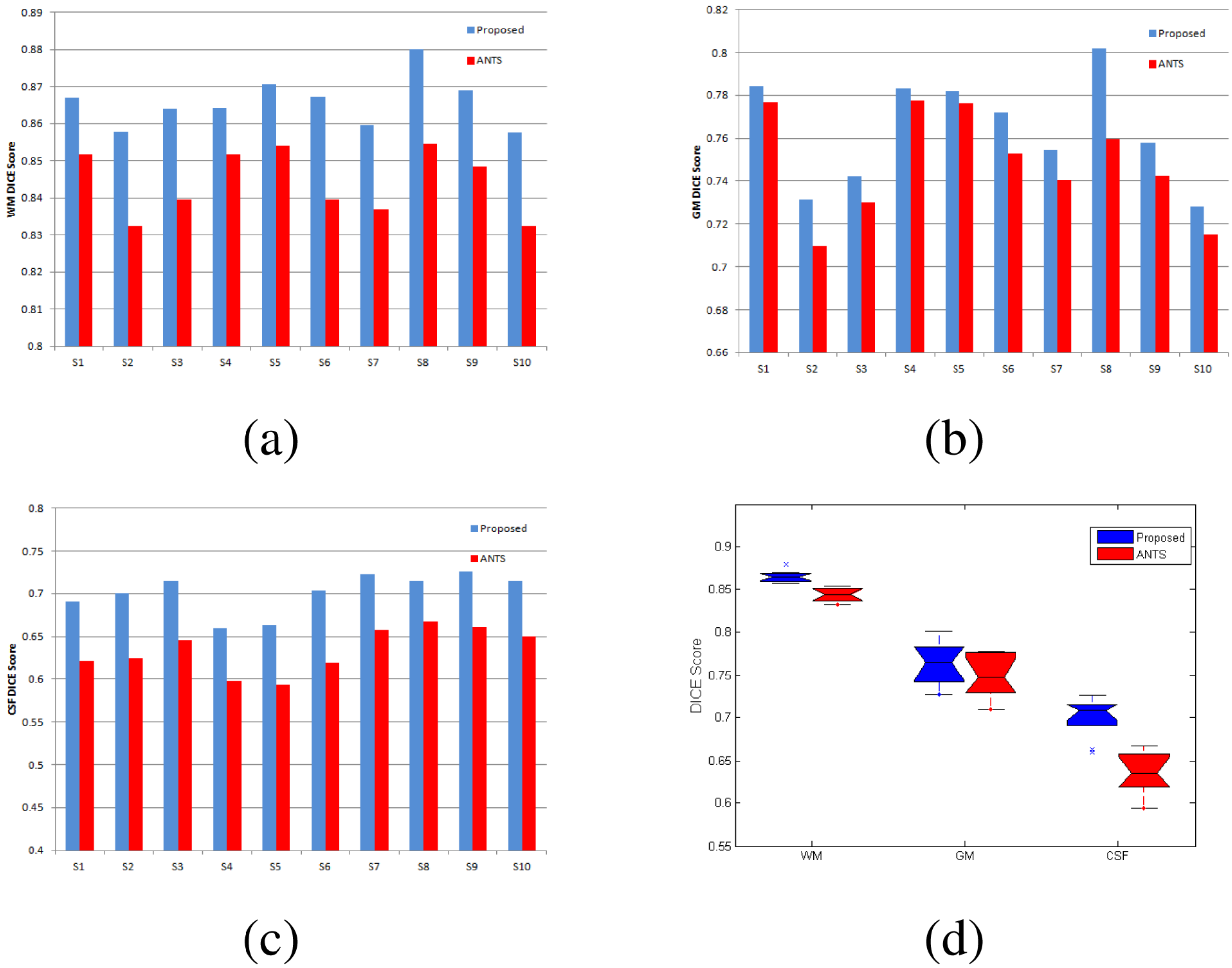

Fig. 3.

The segmentation DICE scores of **(a)** white matter (WM) **(b)** gray matter (GM) and **(c)** cerebrospinal fluid (CSF) for ten subjects in OASIS. **(d)** shows the box plot of the segmentation results.

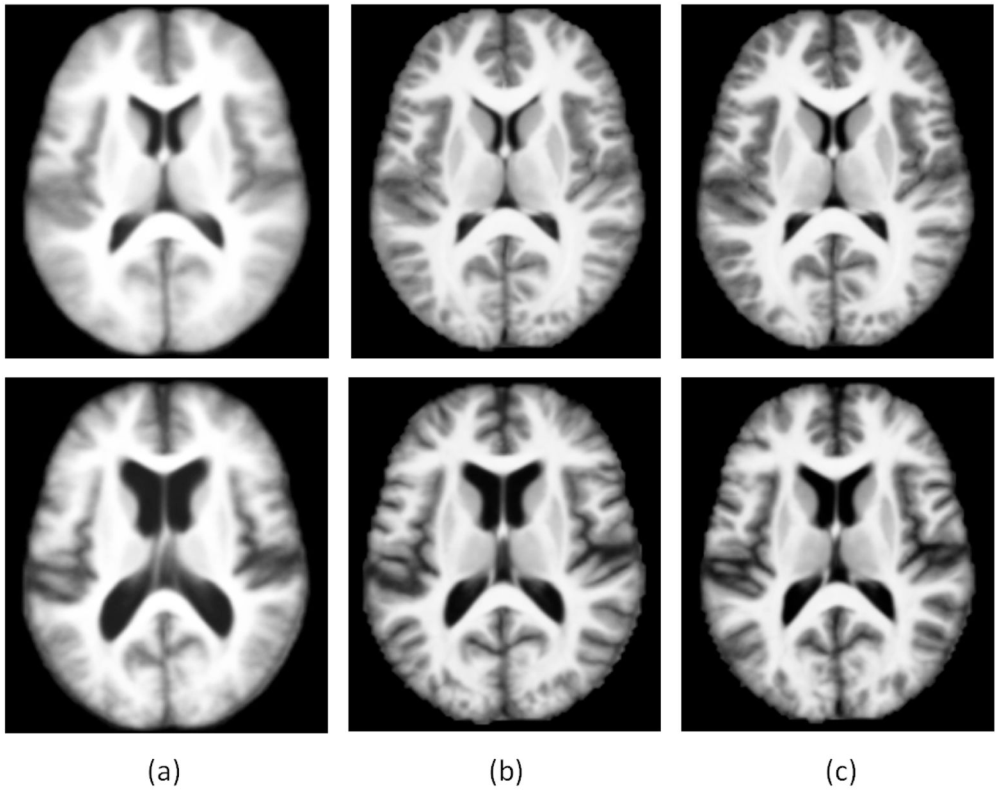

Fig. 4.

Two atlases for OASIS data. **First row**: atlas for young subjects. **Second row**: atlas for older subjects. **(a)**: atlases using iCluster. **(b)**: atlases using our unsupervised algorithm. **(c)**: atlases using our semi-supervised algorithm.

NIH-PA Author Manuscript
NIH-PA Author Manuscript

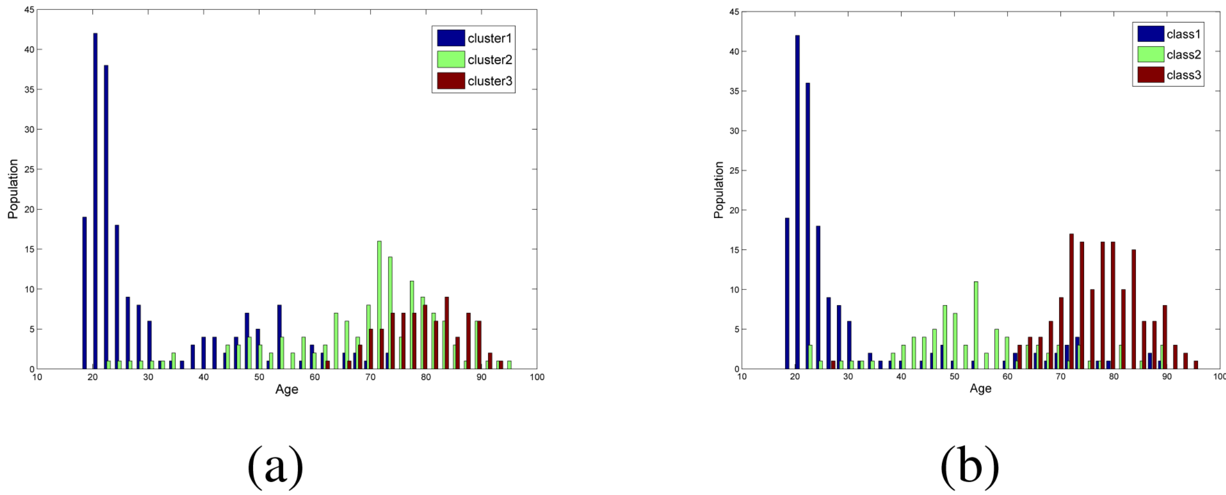

Fig. 5.

Three classes partition. **(a)**: unsupervised method. **(b)**: semi-supervised method. The figure is best viewed in color.

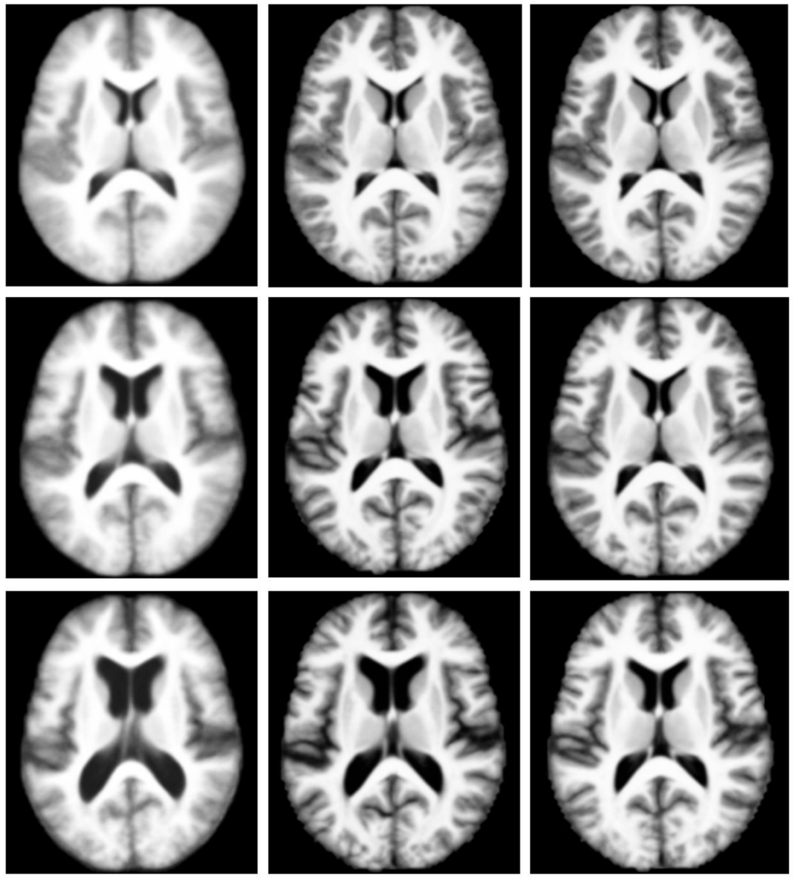

(a) (b) (c)

Fig. 6.

Three atlases for OASIS data. **First row**: atlas for young subjects. **Second row**: atlas for middle aged subjects. **Third row**: atlas for elderly subjects. **(a)**: atlases using iCluster. **(b)**: atlases using our unsupervised algorithm. **(c)**: atlases using our semi-supervised algorithm.

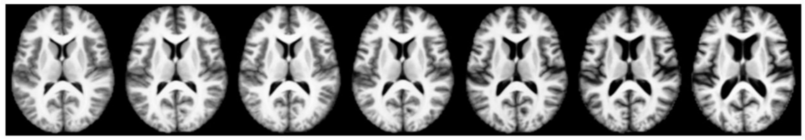

Fig. 7.
Atlases across different ages for subjects in the OASIS data set.

NIH-PA Author Manuscript
NIH-PA Author Manuscript

TABLE I

Means and standard deviations of subject ages for two classes partition

	iCluster	unsupervised	semi-supervised	selected
Class 1	39.1 ± 19.9	37.3 ± 18.7	33.7 ± 17.0	27.7 ± 9.9
Class 2	77.8 ± 9.3	77.0 ± 9.9	75.3 ± 9.6	73.7 ± 10.3

TABLE II

Means and standard deviations of subject ages for three classes partition

	iCluster	unsupervised	semi-supervised	selected
Class 1	31.2 ± 14.5	30.3 ± 13.9	30.0 ± 16.9	23.4 ± 4.4
Class 2	68.9 ± 13.6	67.1 ± 15.2	54.6 ± 14.9	50.4 ± 5.5
Class 3	79.6 ± 7.5	79.6 ± 7.3	77.1 ± 8.5	76.5 ± 8.0

Algorithm 1

Unsupervised graph partition based on spectral clustering

1. Compute similarity matrix **W** and graph Laplacian matrix **L**.
2. Solve the generalized eigenvector problem, $\mathbf{Lu} = \lambda\mathbf{Du}$. Let $\mathbf{u}_1, \ldots, \mathbf{u}_t$ be t eigenvectors corresponding to the smallest eigenvalues and form the matrix $\mathbf{U} = [\mathbf{u}_1, \mathbf{u}_2, \ldots, \mathbf{u}_t] \in \mathrm{IR}^{n\times t}$.
3. Let $\mathbf{y}_i \in \mathrm{IR}^t$ be the i-th row of **U**, where $i = 1, \ldots, n$ and cluster the points $\mathbf{y}_1, \cdots, \mathbf{y}_n$ into t clusters using K-means algorithm.

Algorithm 2

Semi-supervised graph partition

1. Compute similarity matrix **W** and graph Laplacian matrix **L** using both labeled and unlabeled data.
2. Solve the eigenvector problem, $\mathbf{L}\mathbf{u} = \lambda\mathbf{u}$. Let $\mathbf{u}_1, \ldots, \mathbf{u}_p$ be p eigenvectors corresponding to the p smallest eigenvalues.
3. Give s labeled data, we will train t separate two-class classifiers. To estimate the kth classifier f_k, $1 \le k \le t$, we first form a label set $\mathbf{c}_k$ such that the data in class-k have the label value 1 and the data in remaining classes have the label value −1. Then we minimize the following cost function

$$E(\mathbf{a}_k) = \left|\left|\mathbf{U}\mathbf{a}_k - \mathbf{c}_k\right|\right|^2, \quad (8)$$

   and obtain the coefficients $\mathbf{a}_k = (\mathbf{U}^T\mathbf{U})^{-1}\mathbf{U}^T\mathbf{c}_k$ in the linear classifier f_k.
4. We use the coefficients $\mathbf{a}_k = [a_{k1}, \ldots, a_{kp}]^T$, $1 \le k \le t$ computed from step 3 to classify the unlabeled data. For x_i, $i > s$, the label is simply set as $\arg\max_k \sum_{j=1}^{p} a_{kj} u_{ji}$.

Algorithm 3

Multiple atlas construction on image manifolds

---

1 Construct k-NN graph for image data in the quotient space **Q**.

2 Partition the k-NN graph into t subgraphs.

- For unsupervised graph partition, apply the spectral clustering method in Algorithm 1.
- If some image data have labels, apply the semi-supervised graph partition discussed in Algorithm 2.

3 For each of t subgraphs,

- locate the mean on the manifold **M** by solving the convex optimization problem in equation (9).
- generate the image altas by performing the weighted group-wise image registration in equation (11).
